

Synthesis and anomalous magnetic properties of hexagonal CoO nanoparticles

Xuemin He, Huigang Shi*

Key Laboratory for Magnetism and Magnetic Materials of the Ministry of Education, Lanzhou University, Lanzhou 730000, People's Republic of China

ARTICLE INFO

Article history:

Received 29 November 2010
Received in revised form 9 May 2011
Accepted 27 May 2011
Available online 23 June 2011

Keywords:

A. Oxides
B. Chemical synthesis
C. Electron microscopy
D. Magnetic properties

ABSTRACT

CoO nanoparticles in the 38–93 nm range have been prepared by thermal decomposition. The particles were characterized to be pyramid shape with a hexagonal close-packed structure. Their anomalous magnetic behavior includes: (i) vanishing of antiferromagnetic transition around 300 K; (ii) creation of hysteresis below a blocking temperature of 6–11 K; (iii) presence of relatively large moments and coercivities accompany with specific loop shifts at 5 K; and (iv) appearance of an additional small peak located in low field in the electron spin resonance spectrum. Further, the present results provide evidence for the existence of uncompensated surface spins. The coercivity and exchange bias decrease with increasing particle size, indicating a distinct size effect. These observations can be explained by the multisublattice model, in which the reduced coordination of surface spins causes a fundamental change in the magnetic order throughout the total CoO particle.

© 2011 Elsevier Ltd. All rights reserved.

1. Introduction

Bulk CoO is known to be an insulating antiferromagnet with rocksalt cubic structure and Néel temperature of 298 K [1]. In 1961 Néel suggested that small antiferromagnetic nanoparticles (AFN) should exhibit superparamagnetism or weak ferromagnetism [2]. He attributed the permanent magnetic moment to an uncompensated number of spins on two sublattices. Naturally, the magnetic behavior of cubic CoO nanoparticles was widely studied in the next half a century [3–6]. Indeed, large magnetic moments in AFN have been observed [7–10]; however, it also exhibits anomalous magnetic properties such as large coercivities and loop shifts of up to several kOe. This behavior is difficult to understand in terms of 2-sublattice antiferromagnetic ordering which is accepted for bulk materials. According to Kodama and co-workers [11,12], the number of sublattice more than two in AFN, in which these additional sublattices disturb otherwise compensated AF bulk structure and lead to numerous effects including hysteresis and shift of hysteresis loops.

Recently several groups reported the preparation and relevant studies of hexagonal CoO nanocrystals with a wurtzite structure [13–16]. On the one hand, some electronic structure calculations predicted that wurtzite CoO has an antiferromagnetic ground state [17,18]. On the other hand, some experimental studies concluded that no long range magnetic ordering is present in this structure [13,14]. Further, it has been postulated by Dietl et al. [19] that hexagonal CoO nanoparticles with a high Néel temperature

contribute to the observed magnetic moment via uncompensated cobalt spins at the surface. Moreover, Coey and co-workers [20] have suggested that the wurtzite CoO thin films are paramagnetic, which is attributed to the geometric frustration of the antiferromagnetic $\text{Co}^{2+}\text{-O}^{2-}\text{-Co}^{2+}$ superexchange. Obviously, the solution to these conflicting views has become a challenging issue.

Based on the above studies, the peculiarities of structure and even the configuration of magnetic ordering have been analyzed with magnetic resonance [21] or electron spin resonance [22]. Taking into account obvious similarities between CoO and NiO, a strategy which combines resonance technique and multisublattice model may solve the problem mentioned above. Herein we report a facile and reproducible process for the large-scale synthesis of hexagonal CoO nanoparticles. The size of synthesized CoO nanoparticles with pyramid shape can be controlled by changing the precursor concentration. In the present article we focus on the influence of the particle size on the magnetization, coercivity and exchange bias. We present an analysis of the anomalous magnetic properties in terms of a multisublattice model. Finally, the magnetic state of CoO particles was studied by electron spin resonance.

2. Experimental

2.1. Sample preparation

Hexagonal CoO nanoparticles were prepared by the pyrolysis method. In a typical synthesis process, 0.4 g (1.12 mmol) of cobalt(III) acetylacetonate ($\text{Co}(\text{acac})_3$, 98+%) was added to 18.5 ml (56.23 mmol) of oleylamine (OAm, approximate C18-content 80–90%) in a three-necked flask. The bottom of the three-necked flask

* Corresponding author. Tel.: +86 931 8912688; fax: +86 931 8914160.
E-mail address: shihui@lzu.edu.cn (H. Shi).

Table 1

Particle size (D), lattice parameter (a , c), saturation magnetization (M_s), coercivity (H_C) and exchange bias (H_E) for the hexagonal CoO samples synthesized at different precursor concentrations (C).

Sample	C	D (nm)	a and c (Å)	M_s (emu/g)	H_C (Oe)	H_E (Oe)
M1	1/200	38	$a = 3.254(3)$ $c = 5.216(4)$	3.80	845	206
M2	1/150	49	$a = 3.253(1)$ $c = 5.214(2)$	2.94	620	150
M3	1/100	67	$a = 3.251(9)$ $c = 5.213(5)$	2.22	484	83
M4	1/50	93	$a = 3.250(6)$ $c = 5.210(7)$	0.99	357	50

was merged into heat conduction oil for a heating-up. The green slurry was heated at 130 °C (oil bath temperature) for 10 min under an argon atmosphere. Following this dissolution, the green solution was heated up to 210 °C at a rate of 5 °C min⁻¹, and was kept at this temperature for 1 h. Then, the reaction mixture was cooled down to room temperature and a green colloidal solution was formed. The green precipitate was separated upon the addition of ethanol and hexane, centrifuged, and washed using a mixture of ethanol and toluene. Finally, the green CoO nanoparticles (sample M4) were dried in an oven at room temperature, overnight. Under similar reaction conditions, other three CoO samples (M1–M3) with various particle sizes could be produced by simply changing the precursor concentration (the molar ratio of Co(acac)₃ and OAm), as shown in Table 1.

2.2. Characterization

Powder X-ray diffraction (XRD) patterns of samples were recorded from $2\theta = 10\text{--}90^\circ$ on a Philips X'pert diffractometer equipped with a rotating anode and Cu K α radiation ($\lambda = 0.15418$ nm). Scanning electron microscope (SEM) and transmission electron microscope (TEM) images were obtained using a Hitachi S-4800 instrument and a FEI Tecnai G2-F30 instrument, respectively. X-band ($\nu \approx 8.98$ GHz) electron spin resonance (ESR) measurements were carried out on powdered samples in the temperature range of 80–300 K using a JEOL FA200 spectrometer.

2.3. Magnetic measurement

Magnetic measurements were carried out using a superconducting quantum interference device (SQUID) magnetometer (Quantum Design, MPMS-XL). 10 mg of the original aliquots was dispersed in 40 μ l of polyethylene glycol (PEG) solution and then injected into a standard gelatin capsule. In order to measure the exchange bias field, a sample is cooled from 300 to 2 K in an applied magnetic field of 1 T. The field-dependent magnetization is then measured at 5 and 300 K. The saturation magnetization M_s , coercivity H_C and exchange bias H_E are determined from the hysteresis loops after subtracting the linear paramagnetic magnetization of PEG. The H_C and H_E are calculated as $H_C = (|H_{C-}| + |H_{C+}|)/2$ and $H_E = -(H_{C-} + H_{C+})/2$, where H_{C-} and H_{C+} are the negative and positive coercive fields, respectively. The temperature-dependent magnetization $M(T)$ was measured in an applied field of 0.03 T.

3. Results and discussion

Fig. 1 shows typical XRD patterns of the solid samples obtained under different precursor concentrations. It is shown that the four samples are all CoO particles. All the peaks of four patterns are well indexed as wurtzite CoO phase with hexagonal close-packed (hcp)

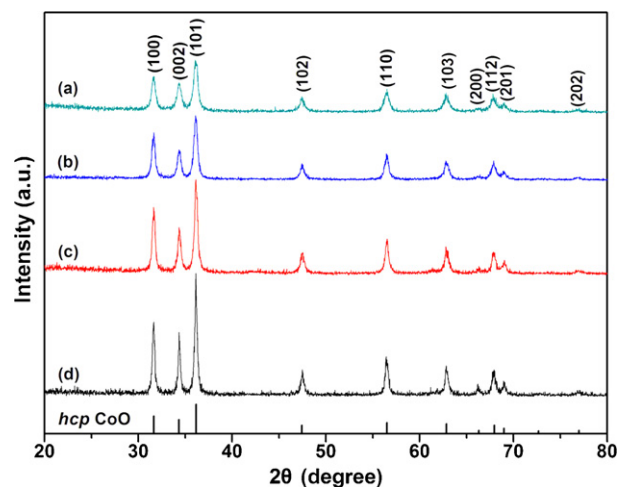


Fig. 1. XRD patterns of CoO nanoparticles formed in different precursor concentrations: (a) 1/200; (b) 1/150; (c) 1/100; (d) 1/50.

structure. Seven obvious Bragg peaks can be assigned to scattering from the (1 0 0), (0 0 2), (1 0 1), (1 0 2), (1 1 0), (1 0 3) and (1 1 2) planes of the CoO crystal lattice, respectively. The peaks are slightly broadened with decreasing precursor concentration. By making use of the line width, the particle size (D) can be estimated using Scherrer formula. The lattice parameter (a , c) increases slightly with the decrease in the particle size in the 38–93 nm range, as shown in Table 1.

Fig. 2 shows the representative SEM images of the as-synthesized CoO particles obtained under different precursor concentrations. It is clear that most CoO particles have pyramid-like shapes. The size distributions of four samples were also shown in Fig. 2a1–d1. Their average particle size was found to be 39.7, 49.3, 64.6 and 94.1 nm, respectively, which was in excellent agreement with the results of XRD analysis. It is obvious that the standard deviations of particle size are less than 10% for all samples. Moreover, the increase of the particle size deteriorates the uniformity of the size distribution. It is reasonable to deduce that the different concentration of oleylamine will cause a different density of organic functional groups on the particle surface, which may be the direct reason for easy control over the particle size and size distribution during the growth process.

Typical TEM images for CoO nanoparticles formed at different precursor concentrations are shown in Fig. 3A–D. It is apparent that the as-synthesized CoO particles are of hexagonal pyramid shaped configuration with various sizes. As the precursor concentration reduced from 1/50 to 1/200, the mean side edge length of CoO particles slightly decreases from 85–105 nm to about 40 nm. As shown in Fig. 3E and F, the hexagonal pyramidal shape can be confirmed by tilting the triangle or hexagon TEM images. The side edge (corresponds to the triangle) length is almost double that of basal edge (corresponds to the hexagon) for the hexagonal CoO particles. Obviously, both particle size and shape are consistent with above SEM analysis. As shown in Fig. 3G, the lattice spacing (d) of 2.60 Å in the triangle image corresponds to the interplanar separation between (0 0 2) lattice planes. While the hexagon image in Fig. 3H shows the lattice fringe images ($d = 2.80$ Å) from the (1 0 0) planes. The corresponding fast Fourier transform (FFT) images of the triangle and hexagon images are shown in the insets of Fig. 3G and H, respectively. The regular dot matrix composed of many bright spots further confirms the hcp structure of CoO particles.

Fig. 4 shows 300 Oe field-cooled (FC) and zero-field-cooled (ZFC) magnetizations as functions of temperature for the CoO

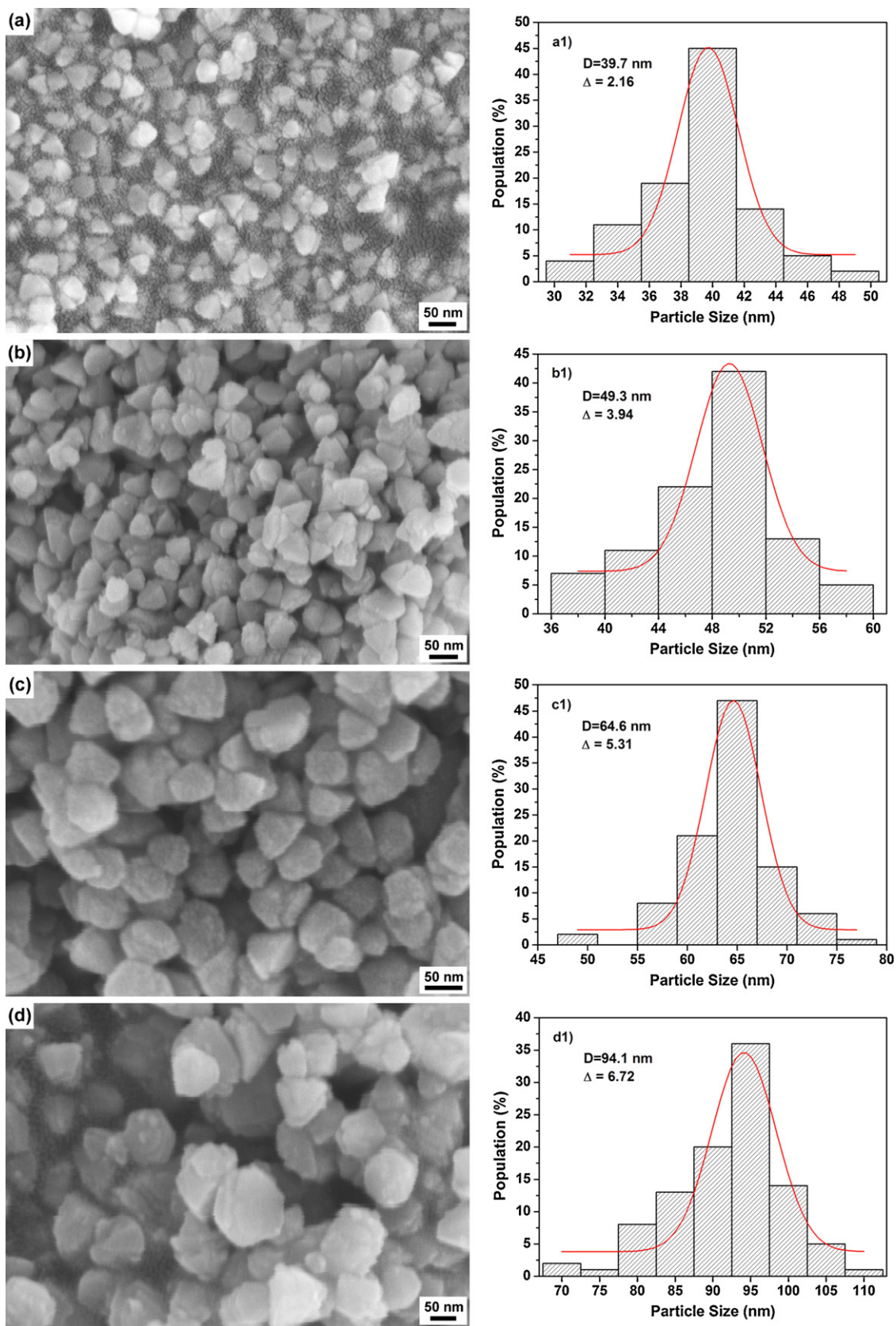


Fig. 2. SEM images and their corresponding size distributions of CoO nanoparticles formed in different precursor concentrations: (a) 1/200; (b) 1/150; (c) 1/100 and (d) 1/50.

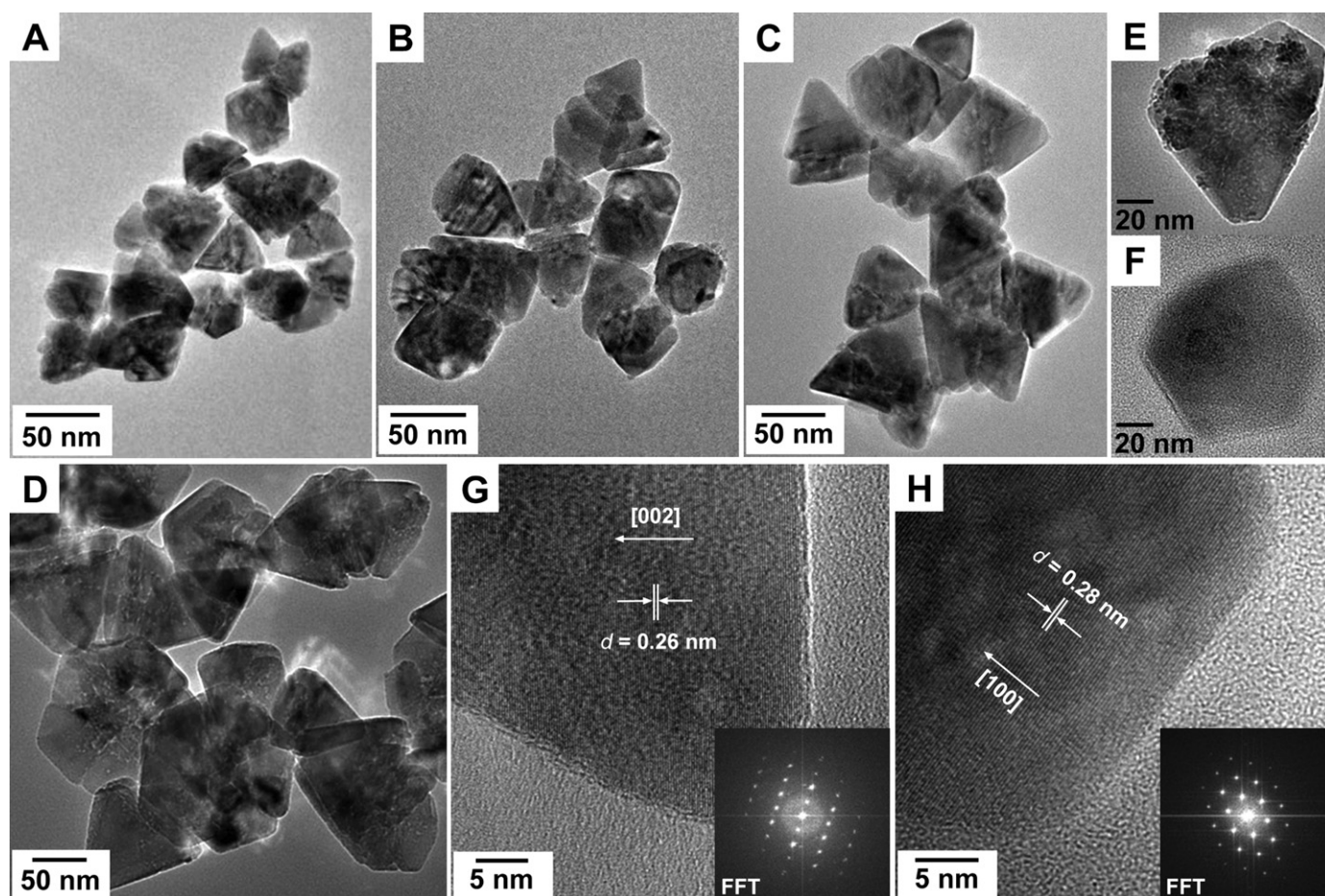


Fig. 3. TEM images of the hexagonal pyramid-shaped CoO nanoparticles formed in different precursor concentrations: (A) 1/200; (B) 1/150; (C) 1/100; (D) 1/50. TEM images of single trigonal (E) and hexagonal (F) nanoparticles. HRTEM lattice fringe images and their corresponding FFT images (see insets) of triangle (G) and hexagon (H) particles.

nanoparticles with various sizes. The field-cooled magnetization M_{FC} increases monotonically with decreasing temperature, and the $M_{FC}(T)$ curves are expected to show a continued rise below the blocking temperature T_B . The zero-field-cooled magnetization M_{ZFC} increases at first and then decreases quickly with the decrease of temperature, and the $M_{ZFC}(T)$ curves exhibit a maximum at T_B . When the temperature is less than T_B , the magnetic moment of individual particles is blocked along one of the anisotropy directions and does not respond to the weak applied field, and hence, the magnetization depends on the magnetic history. This causes the difference in FC and ZFC magnetization. Bulk CoO is known to show an antiferromagnetic transition around 300 K. However, we do not see such a distinct AF transition in our CoO samples. The AF transition is wiped out as the particle size decreases, probably due to ferromagnetic interactions in these nanodimensions. Analogous results were also observed on cubic CoO nanoparticles [4,5]. As can be seen from the insets in Fig. 4, there exhibit a branching phenomenon between the $M_{FC}(T)$ and $M_{ZFC}(T)$ curves. This is attributed to the non-compensation of surface spins. Meanwhile, the blocking temperature of four samples was found to be $\sim 6, 9, 10$ and 11 K, respectively. It is known that T_B depends on interparticle interactions and follows the relationship of $T_B \sim KV$ for diluted samples, where K is the magnetocrystalline anisotropy constant and V is the magnetic volume of a nanoparticle. Further, our CoO samples have the same concentrations, so that the interparticle interactions can be ruled out. It can be deduced that the

magnetic volume V increases, whereas the effective magneto-crystalline anisotropy K decreases with the decrease of total particle size [3,23]. Finally, the comprehensive influence between the two factors leads to the slight change of the blocking temperature from 6 to 11 K.

The insets of Fig. 5 show that the hysteresis loop is superimposed on a large linear background, is exceptionally broad and asymmetric around the origin. Fig. 5 shows the saturating parts of the loops, which can be obtained by subtracting the linear parts from the original hysteresis loops. It is obvious that the magnetization can achieve saturation, and lead to a closed loop. Meanwhile, it clearly showing the presence of coercivity and loop offset. For the four CoO samples with different particle sizes, the specific values of saturation magnetization M_s , coercivity H_C and exchange bias H_E obtained from Fig. 5 are shown in Table 1.

The size dependence of M_s , H_C and H_E are plotted in Fig. 6. Obviously, the M_s , H_C and H_E increase monotonically with decreasing particle size, indicating an obvious size effect. A relative large M_s (3.80 emu/g) can be observed in the 38-nm CoO particles. This is due to the magnetization contribution of the uncompensated surface spins. However, the relative large H_C and H_E are difficult to understand in terms of 2-sublattice antiferromagnetic ordering which is accepted for bulk materials. As has been previously noted on NiO nanoparticles [8,11,24], the observations of large net moments are expected, due to surface termination of the antiferromagnetic structure. Therein the broad and open hysteresis loop was further explained as the

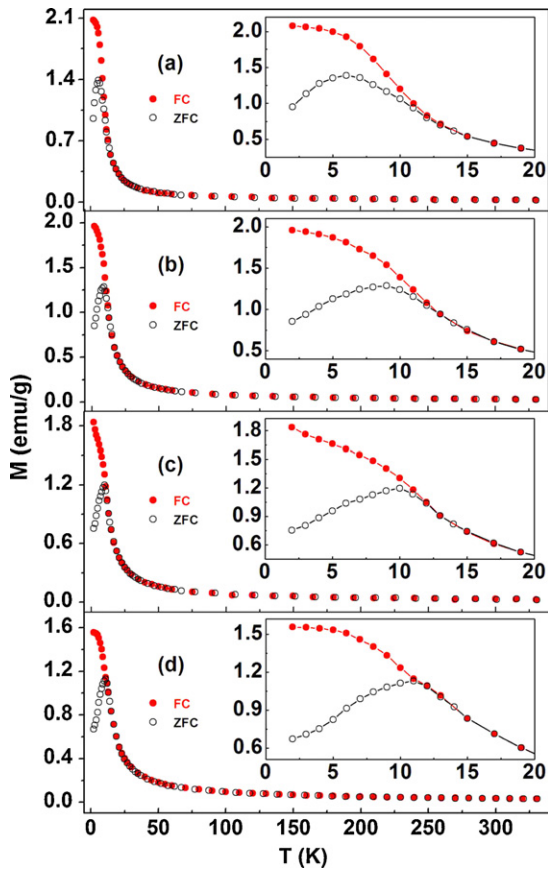


Fig. 4. ZFC and FC (0.03 T) magnetization curves of hexagonal CoO nanoparticles with particle sizes of 38 nm (a), 49 nm (b), 67 nm (c), and 93 nm (d). Insets show greater detail of the same measurements.

result of multiple sublattice formation. This shows that the lower coordination of the surface moments affects the overall antiferromagnetic structure of the entire nanoparticle. According to the multisublattice model [9,11], we expect that the canting of the spins and the number of magnetic sublattices for 38-nm CoO particles is large, and for 93-nm CoO particles is small. As a result, the relatively weak coupling between the sublattices allows a variety of reversal paths for the spins upon cycling the applied field, resulting in large coercivities and loop shifts. In summary, the smaller the particle size, the more the number of the sublattice, and the more helpful to enhance the coercivity and exchange bias.

In order to confirm the exact magnetic state of the CoO nanoparticles, we also performed an ESR spectroscopy study. Fig. 7(a) shows the typical ESR spectra of the 38 nm CoO particles. It is clear that all spectra exhibit an asymmetric broad resonance line. Moreover, an additional small peak located in low field H_{low} can be observed in the total ESR line (H_0 is the resonance field), shown as solid triangles in Fig. 7(b). This additional peak can be considered similar to a ferromagnetic mode. In other words, the resonance observed at H_{low} is attributed to the weak ferromagnetic phase in the hexagonal CoO particles. It is well known that the ESR resonance signal of most bulk antiferromagnets will disappear below the Néel point. For our hexagonal CoO nanoparticles, however, the ESR signal can be detected even at very low temperatures. According to Rivadulla et al. [25], the fact that the resonance line is observable in the AF state is an indication of the existence of canting between multiple sublattices. Obviously, this is in perfect agreement with the results of Kodama et al. [21,22]. Therefore, the ESR study of the CoO nanoparticles has revealed a complicated character of the temperature evolution of the ESR spectra which can be explained in terms of the presence of at least two different magnetic structures. The two resonance lines at H_0 and H_{low} may be attributed to the contributions of intrinsic AF

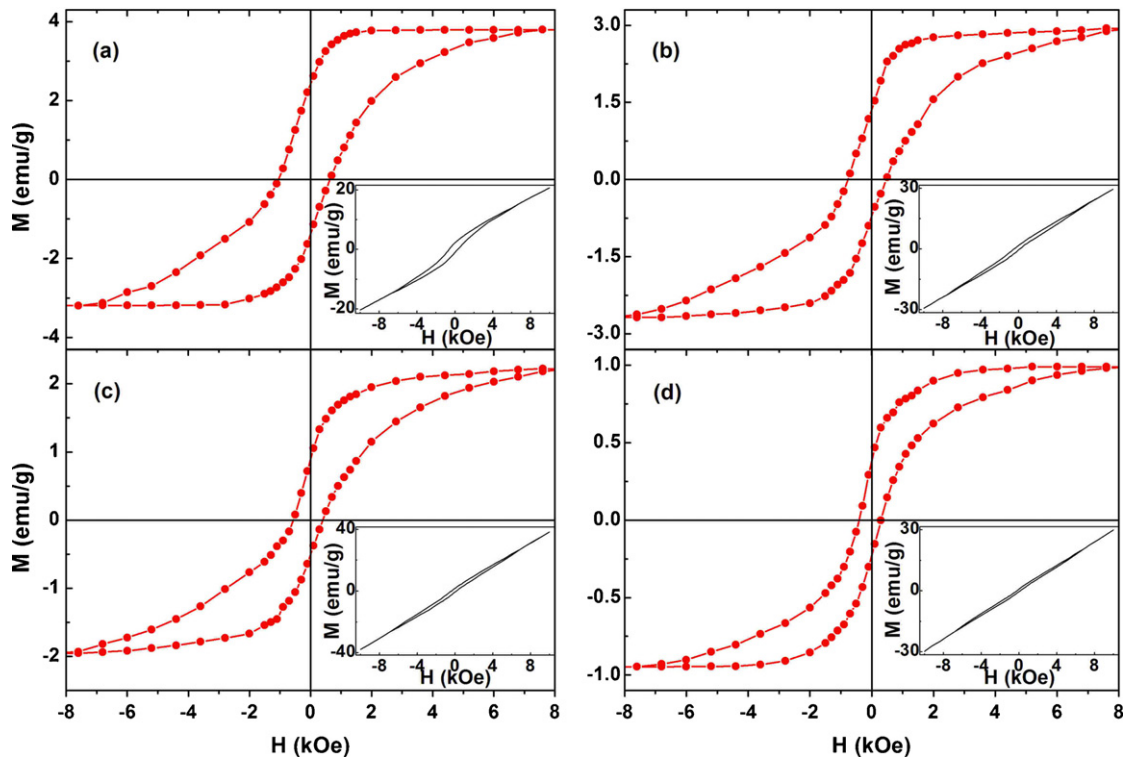


Fig. 5. The saturating parts of the hysteresis loops for the hexagonal CoO nanoparticles with particle sizes of 38 nm (a), 49 nm (b), 67 nm (c), and 93 nm (d), obtained by subtracting the linear parts from the as-measured 5 K magnetization loops (see insets).

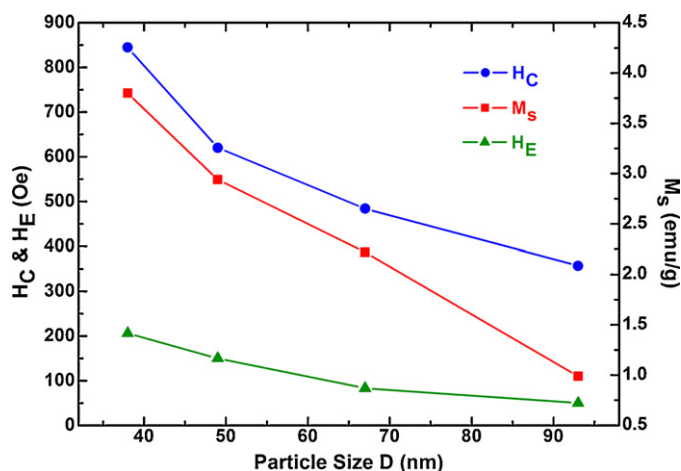


Fig. 6. Size dependence of M_s , H_c and H_E for the hexagonal CoO nanoparticles.

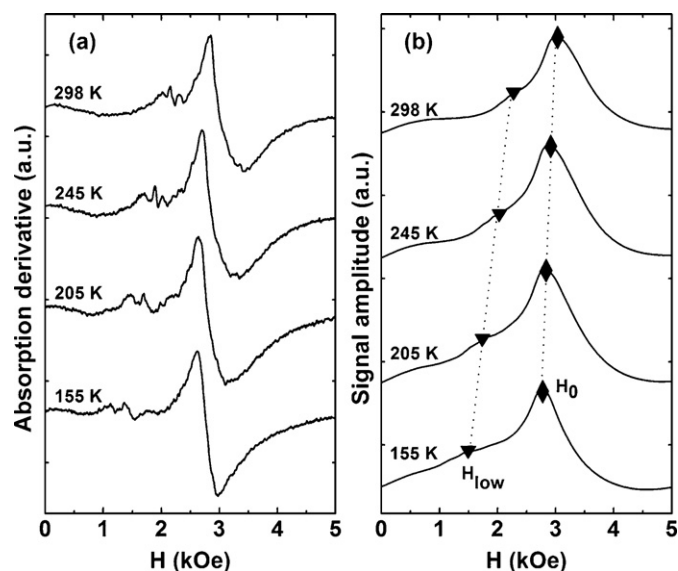


Fig. 7. ESR absorption-derivative spectra (a) and their corresponding integral spectra (b) of the 38 nm CoO nanoparticles for different temperatures.

structure and uncompensated surface spins, respectively. This kind of spectra has been observed for several diluted semiconductor systems [26,27] and antiferromagnetic MnO samples [28].

4. Conclusions

Hexagonal CoO nanoparticles in the size range 38–93 nm were prepared by the thermal decomposition of cobalt acetylacetonate in oleylamine. The hcp-structured CoO nanoparticles are of pyramid configuration, and the particle size increases with increasing precursor concentration. The particles do not exhibit a distinct antiferromagnetic transition around 300 K but instead

show hysteresis at 5 K. Anomalous magnetic properties such as relative large moments, coercivities and loop shifts were observed on hexagonal CoO nanoparticles. The saturation magnetization, coercivity and exchange bias increase monotonically with decreasing particle size, indicating an obvious size effect. According to the multisublattice model, the smaller the particle size, the more the number of the sublattice, and the more helpful to enhance the coercivity and exchange bias. The observed two resonance lines in ESR spectra can be attributed to the contributions of intrinsic antiferromagnetic structure and uncompensated surface spins.

Acknowledgements

The authors would like to express their sincere thanks to Dr. Xiaolong Fan, Prof. Li Xi and Yong Peng for valuable discussion. This work was supported by the National Natural Science Foundation of China (no. 50801033).

References

- [1] C.N.R. Rao, B. Raveau, Transition Metal Oxides, 2nd ed., Wiley-VCH, Weinheim, 1995.
- [2] L. Néel, Compt. Rend. 252 (1961) 4075.
- [3] L.Y. Zhang, D.S. Xue, C.X. Gao, J. Magn. Magn. Mater. 267 (2003) 111–114.
- [4] M. Ghosh, E.V. Sampathkumaran, C.N.R. Rao, Chem. Mater. 17 (2005) 2348–2352.
- [5] D.P. Dutta, G. Sharma, P.K. Manna, A.K. Tyagi, S.M. Yusuf, Nanotechnology 19 (2008) 245609.
- [6] Z.P. Chen, A.Q. Xu, Y. Zhang, N. Gu, Curr. Appl. Phys. 10 (2010) 967–970.
- [7] M. Feyngenson, A. Kou, L.E. Kreno, A.L. Tiano, J.M. Patete, F. Zhang, M.S. Kim, V. Solovyov, S.S. Wong, M.C. Aronson, Phys. Rev. B 81 (2010) 014420.
- [8] S.A. Makhlof, H. Al-Attar, R.H. Kodama, Solid State Commun. 145 (2008) 1–4.
- [9] R.H. Kodama, A.E. Berkowitz, Phys. Rev. B 59 (1999) 6321–6336.
- [10] S.A. Makhlof, F.T. Parker, F.E. Spada, A.E. Berkowitz, J. Appl. Phys. 81 (1997) 5561–5563.
- [11] R.H. Kodama, S.A. Makhlof, A.E. Berkowitz, Phys. Rev. Lett. 79 (1997) 1393–1396.
- [12] A.E. Berkowitz, R.H. Kodama, S.A. Makhlof, F.T. Parker, F.E. Spada, E.J. McNiff Jr., S. Foner, J. Magn. Magn. Mater. 196–197 (1999) 591–594.
- [13] W.S. Seo, J.H. Shim, S.J. Oh, E.K. Lee, N.H. Hur, J.T. Park, J. Am. Chem. Soc. 127 (2005) 6188–6189.
- [14] K. An, N. Lee, J. Park, S.C. Kim, Y. Hwang, J.G. Park, J.Y. Kim, J.H. Park, M.J. Han, J. Yu, T. Hyeon, J. Am. Chem. Soc. 128 (2006) 9753–9760.
- [15] J.F. Liu, S. Yin, H.P. Wu, Y.W. Zeng, X.R. Hu, Y.W. Wang, G.L. Lv, J.Z. Jiang, J. Phys. Chem. B 110 (2006) 21588–21592.
- [16] J.F. Liu, Y. He, W. Chen, G.Q. Zhang, Y.W. Zeng, T. Kikegawa, J.Z. Jiang, J. Phys. Chem. C 111 (2007) 2–5.
- [17] A.S. Risbud, L.P. Snedeker, M.M. Elcombe, A.K. Cheetham, R. Seshadri, Chem. Mater. 17 (2005) 834–838.
- [18] M.J. Han, J. Yu, J. Korean Phys. Soc. 48 (2006) 1496.
- [19] T. Dietl, T. Andrearczyk, A. Lipińska, M. Kieca, M. Tay, Y. Wu, Phys. Rev. B 70 (2004) 235209.
- [20] J. Alaria, N. Cheval, K. Rode, M. Venkatesan, J.M.D. Coey, J. Phys. D: Appl. Phys. 41 (2008) 135004.
- [21] V.V. Pishko, S.L. Gnatchenko, V.V. Tsapenko, R.H. Kodama, S.A. Makhlof, J. Appl. Phys. 93 (2003) 7382–7384.
- [22] M. Rubinstein, R.H. Kodama, S.A. Makhlof, J. Magn. Magn. Mater. 234 (2001) 289–293.
- [23] H.T. Zhang, X.H. Chen, Nanotechnology 16 (2005) 2288–2294.
- [24] E. Winkler, R.D. Zysler, M.V. Mansilla, D. Fiorani, D. Rinaldi, M. Vasilakaki, K.N. Trohidou, Nanotechnology 19 (2008) 185702.
- [25] F. Rivadulla, M. Freita-Alvite, M.A. López-Quintela, L.E. Hueso, D.R. Miguéns, P. Sande, J. Rivas, J. Appl. Phys. 91 (2002) 785–788.
- [26] V. Likodimos, M. Pissas, Phys. Rev. B 76 (2007) 024422.
- [27] E.A. Zvereva, O.A. Savelieva, A.E. Primenko, S.A. Ibragimov, E.I. Slyn'ko, V.E. Slyn'ko, J. Appl. Phys. 108 (2010) 093923.
- [28] M.S. Seehra, G. Srinivasan, J. Appl. Phys. 53 (1982) 8345–8347.